Nanoscale Flow on a Bubble Mattress: Effect of Surface Elasticity

A. Steinberger,[1] C. Cottin-Bizonne,[1] P. Kleimann,[2] and E. Charlaix[1,*]

[1]*Université de Lyon, F-69000, France; Univ. Lyon 1 Laboratoire PMCN; CNRS, UMR 5586; F69622 Villeurbanne Cedex*

[2]*Université de Lyon, F-69000, France; Univ. Lyon 1 INL; F69622 Villeurbanne Cedex*

(Received 12 June 2007; published 31 March 2008)

We present an experimental study of the elastic properties of a superhydrophobic surface in the Cassie regime, due to the gas bubbles trapped at the liquid-solid interface. We use a surface force apparatus to measure the force response to an oscillating drainage flow between a sphere and the surface. We show that the force response allows to determine the surface elasticity without contact, using the liquid film as a probe. The elasticity of the bubble mattress is dominated by the meniscii stiffness, and its determination enables us to probe the shape of these meniscii. Another effect of surface elasticity is to decrease the viscous friction. We show that this effect can be wrongly attributed to rate dependant boundary slippage if elastohydrodynamics is not taken into account.

DOI: 10.1103/PhysRevLett.100.134501 PACS numbers: 47.61.−k, 47.55.D−, 47.85.ld, 68.08.Bc

Superhydrophobic (SH) textured solid surfaces are of interest in many engineering applications [1]. The air trapped in the nonwetting grooves of the surface pattern confers to the composite liquid-solid interface various properties which allow powerful ways to manipulate liquids. In microfluidics, SH surfaces minimize the friction of flows at wall—the trapped air acting as a lubricant—and allow reduced pressure drops in microchannels [2–4]. In self-clearance applications, easy motion of fluid drops is favored by ultralow contact angle hysteresis and weak anchoring of contact lines [5]. In agriculture, the elastic properties of SH surfaces cause the drops of agricultural chemicals to bounce on leaves instead of spread—a drawback to be avoided [6].

In this Letter, we study more specifically the elastic properties of a carpet of bubbles trapped in the holes of a superhydrophobic surface. We present a new method to measure surface elasticity at a distance, using a dynamic flow. For a bubble pattern of micrometric size, we find that the elastic response of bubbles is dominated by their meniscus, with only a small correction arising from the gas compressibility. We also show, as discussed in [7], that bubbles *compliance* reduces the viscous friction of the flow, and that this elastic effect can be wrongly interpreted as a huge boundary slip of the liquid at the wall if not properly taken into account.

The surfaces we use (Fig. 1) are smooth silicon planes etched with holes (radius $a = 0.65 \pm 0.03$ μm, height 3.5 μm) laid on a square lattice of period $L = 1.4$ μm. The microstructure is made by photolithography and electrochemical etching [8]. The plain surfaces are hydrophilic, and wetted by water in the so-called Wenzel regime, i.e., with the liquid filling the holes. Silanized surfaces are superhydrophobic, and water wets them in the Cassie regime, with microbubbles trapped in the holes (advancing contact angle 155°, hysteresis of 9°).

We study a dynamic flow on this ''bubble mattress'' with a dynamic surface force apparatus specifically designed to act as a nanorheometer [9]. A sphere of radius R is immersed in the liquid at a distance D of the surface ($D \ll R$) and oscillated in the normal direction with amplitude h_o (typically 8 Å) at frequency $\omega/2\pi = 19$ Hz. This oscillation creates a drainage flow between the sphere and the surface at the exciting frequency. The device measures the relative distance between the surfaces and the in phase and out of phase amplitudes of the oscillating force acting on the surface, from which the complex force response $G_\omega(D) = -\tilde{F}_\omega(D)/h_o = G'_\omega(D) + iG''_\omega(D)$ is derived. The distance is varied very slowly (5 Å $\cdot$ s^{-1}) and its origin is set at the contact of the sphere and the top of the textured plane, located by a sharp increase of the quasistatic force. The Reynolds number is very small ($Re = h_o\omega\sqrt{RD}/\nu \leq 10^{-7}$, with $\nu = \eta/\rho$ the kinematic viscosity) so that for an incompressible Newtonian liquid and rigid surfaces, the force induced by the flow is purely viscous [$G'_\omega(D > 0) = 0$]. The damping can then be used to study the viscosity and boundary condition of the confined liquid [10]. A nonzero value of $G'_\omega(D)$ obtained with a Newtonian fluid is a signature of elasto-hydrodynamic effects due to surface deformation.

Figure 2(a) shows the components of the force response obtained on the plain hydrophilic surface for a sphere of radius $R = 3.25 \pm 0.05$ mm. The liquid is a water-glycerol

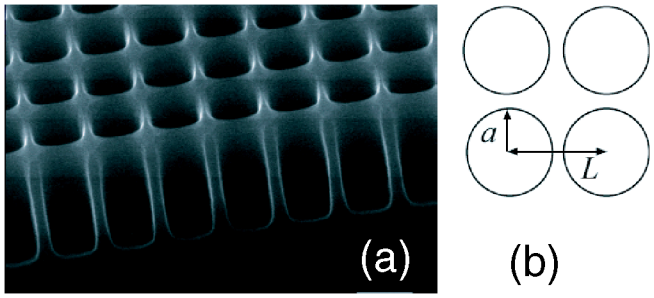

FIG. 1 (color online). SEM picture of the microstructured surfaces. They are modeled as smooth planes with holes of radius 0.65 μm and height 3.5 μm laid on a square lattice of period $L = 1.4$ μm.

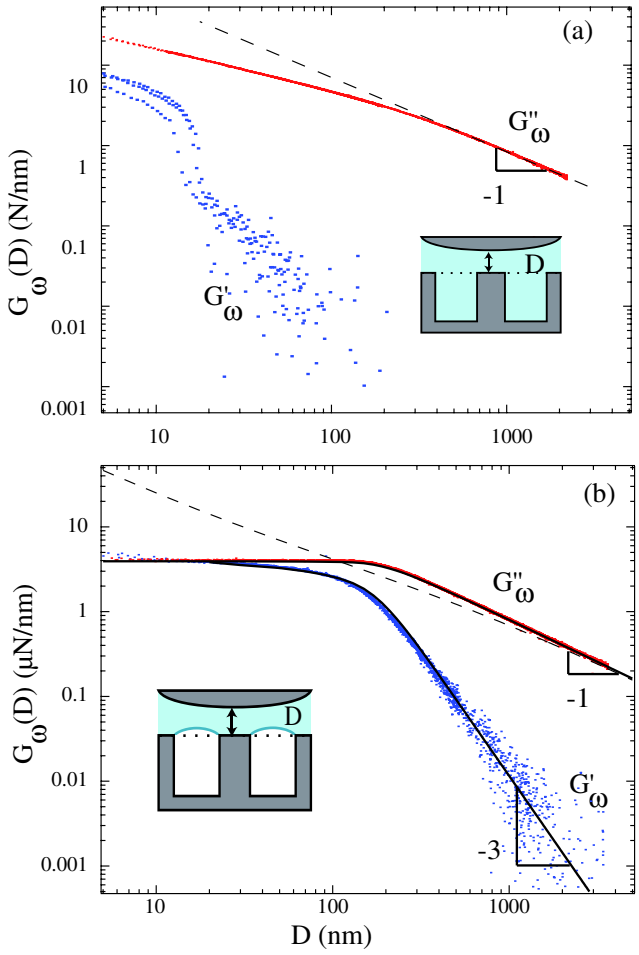

FIG. 2 (color online). Components of the force response $G_\omega(D)$ measured in the Wenzel state (a) and the Cassie state (b) as a function of the distance D between the surfaces. In (a), the dashed line has a slope of -1. In (b), the continuous line is the numerical solution of the EH model computed with a crossover distance $D_c = 211$ nm. For comparison, the dashed line is the damping expected with no elastic effect and a slip length $b = 211$ nm.

solution (78% of glycerol, viscosity 39 ± 1 mPa · s measured with a Ubbelohde viscosimeter), behaving as a Newtonian fluid at the frequency used. Its wetting properties on the patterned surfaces are similar to water so that the liquid fills the holes of the hydrophilic surface. In this Wenzel state, the elastic component $G'_\omega(D)$ is 3 orders of magnitude lower than the viscous component $G''_\omega(D)$, except at short distances comparable to the roughness of the etched silicon (30 nm peak-to-peak measured by atomic force microscopy). Therefore, no significant elastic effect is observed. The viscous damping G''_ω decreases as D^{-1} at large distance, in a way consistent with the Reynolds damping $6\pi\eta\omega R^2/D$ for a flow between a sphere and a plane. The prefactor provides a value of the fluid viscosity $\eta = 39 \pm 2$ mPa · s in very good agreement with the macroscopic determination. At shorter distance, the decrease in friction due to the flow occurring in the holes of the patterned surface becomes visible [11].

On the superhydrophobic surface [Fig. 2(b), sphere radius $R = 3.05 \pm 0.05$ mm, same liquid], the elastic response of the microbubbles trapped in the holes appears clearly. The elastic part of the force response G'_ω has a finite value over the whole range of distances investigated. The viscous damping saturates at a *nonzero* value instead of diverging at small D. This saturation at short distance is due to the bubbles deformation, which essentially compensates for the sphere displacement. At large distance, the viscous damping retrieves the Reynolds D^{-1} scaling with a fluid viscosity $\eta = 39 \pm 2$ mPa · s. For a quantitative analysis, we develop a continuous elasto-hydrodynamic (EH) model describing the flow of a Newtonian and incompressible liquid confined between a rigid oscillating sphere and a flat surface with a local elastic response. The deflection of the surface at distance r from the sphere-plane axis is $\xi(r, t) = K^{-1}P(r, t)$ (Fig. 3) with $P(r, t)$ the local pressure and K the surface stiffness of the square lattice of entrapped bubbles. A lubrication flow is assumed within the liquid film. We use here a no-slip boundary condition, but we have checked that using a partial slip b.c. compatible with the value of the damping measured at large distance does not change significantly the results presented here. The Poiseuille flow and mass balance equations write

$$u(r, t) = -\frac{H^2(r, t)}{12\eta}\frac{\partial P(r, t)}{\partial r}$$

$$\frac{1}{r}\frac{\partial}{\partial r}[rHu(r, t)] = -\frac{\partial H}{\partial t} = -\left(\frac{dh}{dt} + K^{-1}\frac{\partial P(r, t)}{\partial t}\right) \quad (1)$$

with $h(t) = h_o e^{i\omega t}$ the oscillating motion of the sphere, $H(r, t) = D + r^2/2R + h(t) + \xi(t)$ the local thickness of the liquid film, and $u(r, t)$ the thickness-averaged flow velocity. The linearization at small amplitude h_o gives an equation for the complex amplitude $\tilde{P}(r)$ of the pressure

$$-\frac{1}{r}\frac{d}{dr}\left[r\frac{(D + r^2/2R)^3}{12\eta}\frac{d\tilde{P}}{dr}\right] = -i\omega[h_o + K^{-1}\tilde{P}(r)] \quad (2)$$

with the conditions $\tilde{P}(\infty) = 0$ and $(d\tilde{P}/dr)(r = 0) = 0$. With adimensional variables $\tilde{P}' = \tilde{P}/Kh_o$, $x = D/D_c$, $z = Z/D_c$, $D_c = \sqrt{3\eta\omega R/K}$, $Z = D + r^2/2R$, one gets

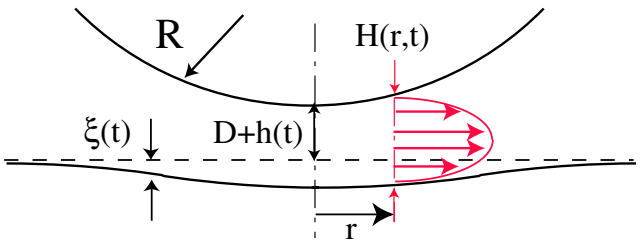

FIG. 3 (color online). Schematics and notations of the EH model.

$$\frac{d}{dz}\left[z^3(z-x)\frac{d\tilde{P}'}{dz}\right] = 2i[1+\tilde{P}'(z)]$$

$$G_\omega(D) = -\frac{1}{h_o}\int_0^\infty 2\pi r dr \tilde{P}(r) = -\frac{6\pi\eta\omega R^2}{D_c}\int_x^\infty \tilde{P}'(z)dz. \quad (3)$$

Solving (3) numerically gives the following scaling laws:

$$G_\omega(D) = \frac{6\pi\eta\omega R^2}{D_c} f(D/D_c)$$
$$f(x) = 1 + j \quad \text{when } x \to 0 \quad (4)$$
$$f(x) = \frac{1}{3x^3} + \frac{j}{x} \quad \text{when } x \to \infty.$$

A simple model for these scaling laws is the following. In the limit of high stiffness K, the Reynolds pressure field $P^o(r) = -j\omega h_o(3\eta R/Z^2)$ obtained from integrating Eq. (2) with $K^{-1} = 0$ is valid if the maximum surface deformation remains small: $\xi = K^{-1}P^o(Z = D) \ll h_o$. This condition defines the large distance limit and the value of D_c. The Reynolds pressure field is approximately constant, equal to $-j\omega h_o(3\eta R/D^2)$ in a region of radius $r \simeq \sqrt{2RD}$ around the sphere apex, and decays as r^{-2} far from it. Therefore, the surface area probed by the flow is $A = 2\pi RD$. In this limit, the viscous force is $F = P^o(D)A = -\lambda(D)j\omega h_o$ with the damping coefficient $\lambda(D) = 6\pi\eta R^2/D$. The surface undergoes a small elastic displacement $\xi \simeq K^{-1}P_{\max} = K^{-1}(F/2\pi RD)$ over the probed area. The equivalent spring stiffness of the elastic surface is thus $k(D) = 2\pi RDK$. The overall force response corresponds to a spring and a dashpot in series

$$G_\omega(D) = \frac{j\lambda\omega k}{(k + j\lambda\omega)} \simeq j\lambda\omega + \lambda^2\omega^2/k. \quad (5)$$

This simple model retrieves both the Reynolds viscous damping and, within a numerical factor, the variation of the elastic response $G'_\omega(D \gg D_c) = 6\pi\eta^2R^3\omega^2K^{-1}/D^3$ at large distances.

In the limit of a soft surface, i.e., $D \ll D_c$, the part of the liquid film whose thickness is lower than D_c cannot drain since the surface cannot sustain the high pressure this would require. Instead, the elastic displacement compensates for the sphere displacement: $\xi \simeq h_o$. This occurs over an area around the sphere apex $2\pi R(D_c - D) \simeq 2\pi RD_c$. The stiffness $k(D)$ thus saturates to $k(D_c)$. Over this area, the pressure in the liquid saturates to its maximum value $P_{\max} = P^o(Z = D_c)$; therefore, the viscous damping also saturates to $\lambda(D = D_c) = k(D_c)/\omega$. The spring-and-dashpot model then retrieves the small distance scaling law (4).

We compare in Fig. 2(b) this continuous elasto-hydrodynamic model to the experimental force response measured in the Cassie regime. A good agreement is found with the scaling laws at small and large distance, with a crossover distance lying in the middle of the range investigated. The variation of the real part as D^{-3} at large distances gives the value of the surface stiffness: $K = 0.95 \pm 0.10\ 10^{12}\ \mathrm{N/m^3}$. This value is then used to compute the full response function of the elasto-hydrodynamic model. This latter provides a good fit of the experimental data over 3 orders of magnitude for the whole range of distances investigated, without other adjustable parameter.

The measured surface stiffness is then compared to the expected surface stiffness of a bubble mattress,

$$K = -L^2\frac{dP_{\mathrm{liq}}}{dV_{\mathrm{bubble}}} \quad (6)$$

where $-dV_{\mathrm{bubble}}/L^2$ is the increase of the film thickness allowed by the bubble deformation and P_{liq} the liquid pressure on the bubble. For the bubble size and the frequency used here, the diffusion of gas in and out from the liquid phase is negligible [7]. Taking into account the capillary pressure drop $P_{\mathrm{cap}} = P_{\mathrm{liq}} - P_{\mathrm{gas}}$ across the meniscus, the compressibility of a single bubble is

$$\frac{dP_{\mathrm{liq}}}{dV_{\mathrm{bubble}}} = \frac{dP_{\mathrm{gas}}}{dV_{\mathrm{bubble}}} + \frac{dP_{\mathrm{cap}}}{dV_{\mathrm{bubble}}} = -\frac{1}{\aleph_g V_{\mathrm{bubble}}} - \frac{2\gamma}{\pi a^4}\cos\theta(1+\cos\theta)^2 \quad (7)$$

with $\aleph_g$ the bubble gas compressibility, $\gamma = 63 \pm 3\ \mathrm{mN/m}$ the liquid-gas surface tension, and θ the angle formed by the spherical-cap meniscus with the plane surface [12]. It is shown in Fig. 4 that with the micrometric hole size of our surface, the meniscus contribution dominates over the gas compressibility. The magnitude of the measured surface stiffness is in good agreement with the expected stiffness of the bubble mattress. More specifically, with the numerical values $a = 0.65\ \mu\mathrm{m}$ and

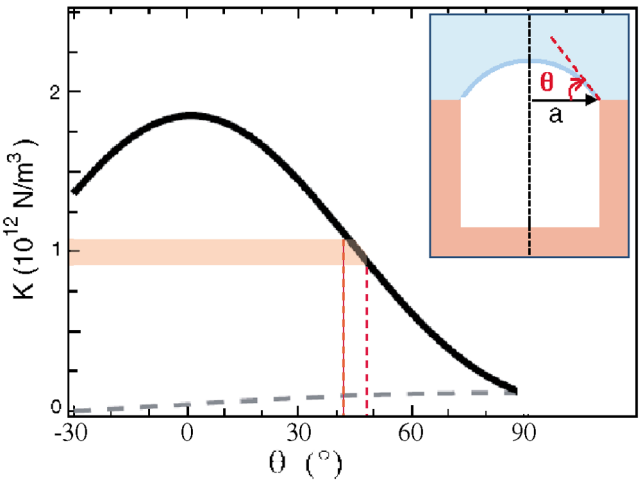

FIG. 4 (color online). Expected stiffness K of a bubble mattress calculated from Eq. (7). The bubbles are trapped in a square lattice of cylindrical holes. Their meniscus protrude with an angle θ above the solid surface. The dashed line plots the contribution of the gas compressibility to the overall stiffness. The rectangle is the surface stiffness measured with its error bar.

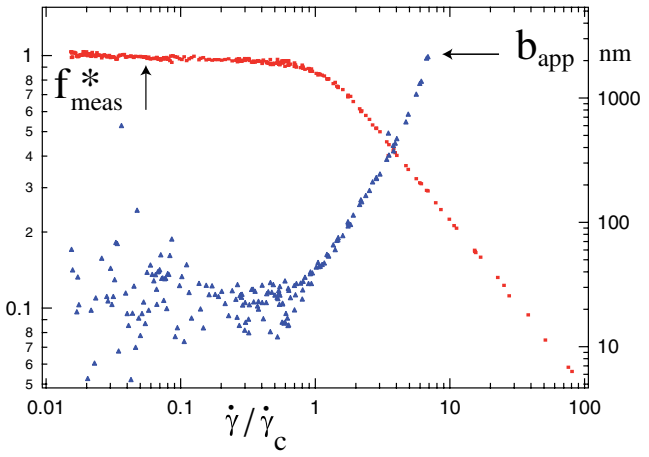

FIG. 5 (color online). Left axis: ratio f^*_{meas} of the measured damping G''_ω normalized to the Reynolds damping $6\pi\eta\omega R^2/D$ as a function of the normalized shear rate at wall $\dot\gamma/\dot\gamma_c = (D_c/D)^{3/2}$. Right axis: *apparent* slip length b_{app} derived from f^*_{meas} assuming no elastic effect and a partial slip boundary condition.

$L = 1.4\ \mu$m, we find that the measured stiffness in this experiment corresponds to protruding meniscii forming an angle $\theta = 46° \pm 6°$ with the surface plane. This protruding configuration is likely due to the rounded geometry of the hole edges on which the meniscus merges to the substrate. It is of interest to mention that the expected meniscus stiffness does not depend on the sign of θ, i.e., is similar for a protruding or intruding meniscus. However, we have to eliminate the possibility of an intruding (negative) angle, since $\theta < -30°$ would lead to a negative pressure in the gas phase.

In conclusion, we show here a new method to measure surface elastic properties at a nanoscale, at a distance, and without mechanical contact. This method can be applied to a wide range of elastic surfaces, by tuning the liquid viscosity. It has interesting applications for fragile surfaces on which direct contact should be avoided, or complex surfaces which properties can be affected by the proximity of a mechanical probe, such as ultrathin polymer films [13,14]. We have also shown that the elastic properties of a carpet of micrometric bubbles is determined by the deformation of their free surface. The measurement of the surface elasticity thus allows to probe the shape of the meniscii.

Finally, in the spirit of [7], we want to comment on the importance of surface elasticity effects for the study of liquid friction at surfaces, and boundary hydrodynamics in general. As shown by the saturation of the damping in Fig. 2(b), a consequence of surface elasticity is to reduce the overall viscous friction of a flow. This reduction of friction is *not* due to liquid slippage at the solid surface, but to the fact that surface deformation allows more space for the flow. As a result, if not taken properly into account, the existence of a finite surface elasticity can be wrongly attributed to liquid slippage at the surface. More important, because the amplitude of surface deformation depends on the viscous stress, the *apparent* boundary effect depends on the shear rate. We illustrate this effect in Fig. 5 by plotting the *apparent* slip length that would be obtained *if* the elasto-hydrodynamic force response were wrongly interpreted in terms of boundary slippage. This apparent slip length b_{app} is derived point-by-point from the ratio $f^*_{\mathrm{meas}} = G''_\omega(D)/(6\pi\eta\omega R^2/D)$ of the measured viscous response to the Reynolds force, by comparing it to the theoretical value $f^*_{\mathrm{th}}(b_{\mathrm{app}}/D)$ [15]. When $D > D_c$, the EH effects are negligible and the slip length has a low limit value corresponding to the actual boundary condition on the Cassie surface [11]. However, when $D < D_c$, the surface deflection is significant, and the *apparent* slip length increases by orders of magnitude. This is plotted in Fig. 5 as a function of the shear rate at wall $\dot\gamma = 1.38 h_o\omega\sqrt{R}/D^{3/2}$ normalized by the critical shear rate $\dot\gamma_c = \dot\gamma(D_c)$. Rate-dependent slip effects with a threshold shear rate have indeed been reported in literature [16]. Our results show the necessity to control sharply surface elasticity effects in order to investigate rate effects in boundary conditions.

We thank P. Y. Verilhac for helpful contribution. This work was financially supported by the ANR P-Nano.

*charlaix@lpmcn.univ-lyon1.fr

[1] D. Quéré, Rep. Prog. Phys. **68**, 2495 (2005).
[2] C. Cottin-Bizonne *et al.*, Nat. Mater. **2**, 237 (2003).
[3] J. Ou and J. Rohstein, Phys. Fluids **16**, 4635 (2004).
[4] P. Joseph *et al.*, Phys. Rev. Lett. **97**, 156104 (2006).
[5] D. Quéré, A. Lafuma, and J. Bico, Nanotechnology **14**, 1109 (2003).
[6] D. Richard, C. Clanet, and D. Quéré, Nature (London) **417**, 811 (2002).
[7] E. Lauga and H. Brenner, Phys. Rev. E **70**, 026311 (2004).
[8] P. Kleimann, X. Badel, and J. Linros, Appl. Phys. Lett. **86**, 183108 (2005).
[9] F. Restagno *et al.*, Rev. Sci. Instrum. **73**, 2292 (2002).
[10] C. Cottin-Bizonne, B. Cross, A. Steinberger, and E. Charlaix, Phys. Rev. Lett. **94**, 056102 (2005).
[11] A. Steinberger *et al.*, Nat. Mater. **6**, 665 (2007).
[12] E. Charlaix and H. Gayvallet, J. Phys. II **2**, 2025 (1992).
[13] Y. Sun, B. Akhremitchev, and G. Walker, Langmuir **20**, 5837 (2004).
[14] H. Bodiguel and C. Fretigny, Phys. Rev. Lett. **97**, 266105 (2006).
[15] O. I. Vinogradova, Langmuir **11**, 2213 (1995).
[16] Y. Zhu and S. Granick, Phys. Rev. Lett. **87**, 096105 (2001).